Overview of toroidal momentum transport

2011 Nucl. Fusion 51 094027

(http://iopscience.iop.org/0029-5515/51/9/094027)

IOP Publishing and International Atomic Energy Agency Nuclear Fusion
Nucl. Fusion **51** (2011) 094027 (13pp) doi:10.1088/0029-5515/51/9/094027

Overview of toroidal momentum transport

A.G. Peeters[1], C. Angioni[2], A. Bortolon[3], Y. Camenen[4], F.J. Casson[5], B. Duval[6], L. Fiederspiel[6], W.A. Hornsby[1], Y. Idomura[7], T. Hein[2], N. Kluy[2], P. Mantica[8], F.I. Parra[9], A.P. Snodin[5], G. Szepesi[5], D. Strintzi[2], T.Tala[10], G. Tardini[2], P. de Vries[11] and J. Weiland[12]

[1] University of Bayreuth, Physics Department, 95440 Bayreuth, Germany
[2] Max Planck Institut (IPP) Euratom assoc., Boltzmannstrasse 2 85748 Garching, Germany
[3] University of California Irvine, Physics and Astronomy Department, CA 92697, USA
[4] IIFS, CNRS-Université de Provence, Marseille, France
[5] University of Warwick, Physics Department, sCV7 4AL Coventry, UK
[6] CRPP-EPFL, Euratom associated, CH-1015 Switzerland
[7] Japan Atomic Energy Agency, Tokyo 110-0015, Japan
[8] Istituto di Fisica del Plasma 'P.Caldirola', Associazione Euratom-ENEA-CNR, Milano, Italy
[9] Rudolf Peierls Centre for Theoretical Physics, University of Oxford, Oxford, OX1 3NP, UK
[10] Association EURATOM-Tekes, VTT, PO Box 1000, FIN-02044 VTT, Finland
[11] FOM Institute Rijnhuizen, Association EURATOM-FOM, Nieuwegein, The Netherlands
[12] Chalmers University of Technology and Euratom-VR Association, Göteborg Sweden

E-mail: arthur.peeters(at)uni-bayreuth.de

Received 22 January 2011, accepted for publication 21 July 2011
Published 31 August 2011
Online at stacks.iop.org/NF/51/094027

Abstract
Toroidal momentum transport mechanisms are reviewed and put in a broader perspective. The generation of a finite momentum flux is closely related to the breaking of symmetry (parity) along the field. The symmetry argument allows for the systematic identification of possible transport mechanisms. Those that appear to lowest order in the normalized Larmor radius (the diagonal part, Coriolis pinch, $E \times B$ shearing, particle flux, and up–down asymmetric equilibria) are reasonably well understood. At higher order, expected to be of importance in the plasma edge, the theory is still under development.

(Some figures in this article are in colour only in the electronic version)

1. Introduction

Plasma rotation plays a key role in regulating turbulence and has a beneficial effect on energy confinement in fusion devices through $E \times B$ shearing [1, 2]. Furthermore, a sufficiently large rotation can stabilize the resistive wall mode [3, 4]. Toroidal rotation plays a special role in tokamaks due to the symmetry of the device. This symmetry leaves the toroidal angular rotation, in contrast to the poloidal rotation, undamped and, consequently, the toroidal rotation can attain values much in excess of the poloidal rotation. Toroidal velocity shear translates into both $E \times B$ shear, perpendicular to the background magnetic field, and parallel velocity shear. While the former is beneficial for confinement, the latter can enhance turbulent transport, since in toroidal geometry the parallel velocity gradient adds a drive to the ion temperature gradient (ITG) mode [5–7]. It is largely the ratio of the poloidal to the toroidal magnetic field strength $B_p/B_t \approx \epsilon/q$ that determines the relative strength of these two mechanisms. For sufficiently large B_p/B_t the $E \times B$ shear dominates and turbulence is suppressed.

Early experimental observations on momentum transport [8–17] and theoretical investigations into anomalous transport [18] suggest a strong coupling of ion heat and momentum transport, with the diagonal transport coefficients being of similar magnitude. These experiments were performed using neutral beam heating (NBH) which exerts a large torque on the plasma, and the understanding was that without external momentum input, the plasma rotation would be negligible. This picture radically changed through the discovery of the so-called intrinsic rotation [19–29], i.e. the finite rotation a plasma develops without an external toroidal torque. The

intrinsic rotation is of particular interest to a reactor plasma for which the external torque will be small. Subsequently, mechanisms of toroidal momentum transport have attracted much recent attention in the community, leading to a very rapid development in theory and modelling. This paper will give an overview of the developments in this relatively new area and puts them in a global perspective. We will concentrate on flow generation in a toroidally symmetric device, the interesting physics connected with the breaking of toroidal symmetry being discussed in a complementary overview [30]. The paper has partly the nature of a review paper, but also contains a substantial amount of new material.

Since toroidal angular momentum is conserved, its evolution equation can be written in conservative form [31–35]

$$\sum_{\rm sp} \frac{\partial \{n_{\rm sp} m_{\rm sp} R^2 \Omega\}}{\partial t} + \nabla \cdot \{\mathbf{\Gamma}_\varphi\} = \{S_\varphi\}, \tag{1}$$

where $m_{\rm sp}$ ($n_{\rm sp}$) is the particle mass (density) and the sum is over all species. R is the major radius, Ω is the angular rotation frequency, $\mathbf{\Gamma}_\varphi$ is the angular toroidal momentum flux, S_φ is the external torque, and the brackets $\{\ \}$ denote the flux surface average. In [35] the gyro-kinetic evolution equation is derived directly from the Lagrangian description in a general form. Various approximations can be made without violating momentum conservation, provided the approximations are made at the level of the Lagrangian / Hamiltonian. The relevant momentum flux and, indeed, the appropriate approximation of the toroidal angular momentum depend on the choice of the Lagrangian. For the present discussion it is sufficient to consider the long wavelength limit of the electro-magnetic case (neglecting magnetic field compression effects). The momentum equation then takes the form [35]

$$\begin{aligned}\frac{\partial}{\partial t}\left[\sum_{\rm sp}\left\{m_{\rm sp} n_{\rm sp} R v_{E\rm t} + \frac{R B_{\rm t}}{B}\int m_{\rm sp} v_\parallel f_{\rm sp} {\rm d}^3\boldsymbol{v}\right\}\right] \\ + \frac{1}{V'}\frac{\partial}{\partial r}\left[V'\left\{\frac{R B_{\rm t}}{B}\sum_{\rm sp}\int m_{\rm sp} v_\parallel \left(v_{Er} + v_\parallel \frac{\tilde{B}_r}{B}\right) f_{\rm sp} {\rm d}^3\boldsymbol{v}\right.\right. \\ \left.\left. + \sum_{\rm sp} m_{\rm sp} n_{\rm sp} R v_{E\rm t} v_{Er} - \frac{R}{\mu_0}\tilde{B}_{\rm t}\tilde{B}_r\right\}\right] = 0,\end{aligned} \tag{2}$$

where only the lowest order (in the normalized Larmor radius $\rho_* = \rho/R$) terms have been kept, $Z_{\rm sp}$ is species charge number, and $f_{\rm sp}(\boldsymbol{R}, v_\parallel, \mu)$ the distribution function. The subscript t (r) denotes the toroidal (radial) component, $v_E = \boldsymbol{b}\times\nabla\phi/B$ is the $E\times B$ velocity, with ϕ the (perturbed) electric potential. $\tilde{\boldsymbol{B}} = \nabla\times(A_\parallel \boldsymbol{b})$ is the perturbed magnetic field, with $A_\parallel$ the component of the perturbed vector potential along the background magnetic field ($\boldsymbol{B} = B\boldsymbol{b}$). The minor radius r is a flux surface label in the case of general geometry, V the volume enclosed by the flux surface, and $V' = \partial V/\partial r$.

The term under the time derivative is the flux surface averaged toroidal angular momentum, consisting of the toroidal component of the $E\times B$ velocity and the toroidal component of the parallel momentum. Likewise, the toroidal angular momentum flux is due to the transport of parallel and perpendicular momentum. The flux connected with the parallel component is represented by the integral over the perturbed distribution f and is due to the radial component of the $E\times B$ velocity (v_{Er}) and the radial motion due to the parallel streaming along perturbed field lines ($v_\parallel \tilde{B}_r/B$). The flux connected with the perpendicular momentum is due to the Reynolds stress ($m_{\rm sp} n_{\rm sp} v_{E\rm t} v_{Er}$ the transport of the toroidal component of the $E\times B$ velocity by the radial component) and the Maxwell stress ($\tilde{B}_{\rm t}\tilde{B}_r/\mu_0$ connected with the Lorentz Force $\tilde{\boldsymbol{J}}\times\tilde{\boldsymbol{B}}$). The three contributions to the flux surface averaged momentum flux that appear in the equation above can be ordered using the gyro-kinetic ordering ($\tilde{n}/n = \mathcal{O}(\rho_*)$, $e\phi/T = \mathcal{O}(\rho_*)$, $ev_{\rm th}A_\parallel/T = \mathcal{O}(\rho_*\sqrt{\beta})$), to obtain $\rho_*^2 R m n v_{\rm th}^2 (k_y\rho)\times[1 : B_{\rm p}(k_r\rho)/B : B_{\rm p}(k_r\rho)/B]$, where k_y (k_r) is the bi-normal (radial) wave vector. The Reynolds and Maxwell stresses are formally of the same order in ρ_* compared with the parallel momentum flux, but are smaller by a factor $B_{\rm p}(k_r\rho)/B$. For fully developed turbulence the dominant mode often satisfies $k_r\rho \approx 0.1$, and the small ratio $B_{\rm p}/B$ then results in Reynolds and Maxwell stresses that are of the order of one percent compared with the radial component of the parallel momentum flux. For this reason the radial transport of toroidal momentum is often approximated by the latter contribution, an approximation that will also be frequently used in this paper.

It is to be noted that a large part of the work on momentum transport is based on the δf approximation [36, 37] in which the parallel velocity nonlinearity is neglected, since it is one order smaller in ρ_* compared with the leading order terms. This approach does not guarantee momentum conservation as it is not derived directly from a Lagrangian approach. Flux tube simulations are nevertheless expected to yield the correct flux to lowest order in ρ_*, since in this type of simulations the background rotation is not dynamically evolving, but rather the flux is calculated for a given rotation profile. In the local approximation the turbulence is homogeneous, and the periodic radial boundary conditions allow for a stationary background rotation that is consistent with the radial momentum flux since the divergence of this flux is, on average, zero. The calculation of the momentum flux in the δf approximation is similar to that of the energy flux which is calculated at fixed temperature gradient, with the model not conserving energy to all orders in ρ_*. The neglect of the parallel velocity nonlinearity, however, does mean that the δf approximation cannot be used to calculate all higher order (in ρ_*) contributions to the momentum flux.

2. Symmetry breaking

Toroidal momentum transport is related to a breaking of symmetry [5, 38]. To demonstrate this we seek a transformation that flips the sign of the radial momentum flux, while leaving the gyro-kinetic equation invariant. If such a transformation exists, the gyro-kinetic equation allows for equivalent solutions which have the opposite sign of the momentum flux. Linearly, these solutions would grow with equal growth rate, and nonlinearly they would occur with equal probability. It follows that when the symmetry is satisfied, the net momentum flux is zero. Note that for the turbulent state the statement above is satisfied in a statistical sense only, i.e. the momentum flux will fluctuate around zero rather than have a zero value at all time. Since symmetry implies zero momentum flux, it directly determines under which conditions toroidal

momentum can be transported. All transport mechanisms can be identified through their breaking of the symmetry.

The symmetry argument is briefly outlined for the electro-static collisionless case. The extension to the collisional electro-magnetic case will then be discussed at the end of the section. Starting point of the derivation will also be the momentum flux due to the radial transport of the parallel momentum

$$\Gamma^r_\parallel = -\sum_{\rm sp} \frac{RB_{\rm t}}{B} \int {\rm d}^3\boldsymbol{v}\, \frac{1}{B} \frac{\partial \langle\phi\rangle}{\partial y} m_{\rm sp} v_\parallel f_{\rm sp}, \tag{3}$$

with the other contributions being discussed at the end of the section. A change in sign of the momentum flux given above can be obtained through a change in sign of the parallel velocity ($v_\parallel \rightarrow -v_\parallel$). With the first transformation defined, all the terms in the gyro-kinetic equation are investigated. This leads to additional transformations as well as conditions that must be satisfied for the gyro-kinetic equation to remain invariant.

To lowest order, in the normalized Larmor radius $\rho_* = \rho/R$, the equation for the perturbed distribution (f) satisfies

$$\begin{aligned}
&\frac{\partial f}{\partial t} + v_\parallel \frac{\partial f}{\partial s} + (\boldsymbol{v}_D + \boldsymbol{v}_E + \boldsymbol{v}_{EB}) \cdot \nabla f - \mu \frac{\partial B}{\partial s} \frac{\partial f}{\partial v_\parallel} \\
&\quad = -\frac{1}{B} \frac{\partial \langle\phi\rangle}{\partial y} \left[\frac{1}{L_n} + \left(\frac{mv^2}{2T} - \frac{3}{2} \right) \frac{1}{L_T} \right. \\
&\qquad \left. - \frac{m v_\parallel - RB_{\rm t}\Omega/B}{T} \frac{RB_{\rm t}\nabla\Omega}{B} \right] F_{\rm M} \\
&\qquad - \left(v_\parallel \frac{\partial \langle\phi\rangle}{\partial s} + \boldsymbol{v}_D \cdot \nabla \langle\phi\rangle \right) \frac{Ze}{T} F_{\rm M},
\end{aligned} \tag{4}$$

where field aligned coordinates (r, y, s) are used, with r the radial, y the bi-normal, and s the coordinate along the field. The parallel velocity ($v_\parallel$) and magnetic moment (μ) are used as velocity space coordinates, $\boldsymbol{v}_D$ is the drift due to the inhomogeneous magnetic field, and $\boldsymbol{v}_E = \boldsymbol{b} \times \nabla\langle\phi\rangle/B$ ($\boldsymbol{v}_{EB}$) is the $E \times B$ drift due to fluctuating (background) potential $\langle\phi\rangle$ (Φ), with the angle brackets $\langle\rangle$ denoting the gyro average. $F_{\rm M}$ is the Maxwell distribution shifted in the parallel velocity by the background parallel velocity $RB_{\rm t}\Omega/B$, and the gradients of density and temperature are represented by $1/L_n \equiv -\nabla n/n$ and $1/L_T \equiv -\nabla T/T$. The equation above is derived for a toroidally rotating plasma with a background angular frequency Ω. Diamagnetic and neo-classical equilibrium effects are neglected in agreement with the lowest order ρ_* approximation.

From the parallel streaming term (second term in equation (4)), using $v_\parallel \rightarrow -v_\parallel$, it is clear that the gyro-kinetic equation is invariant only when the coordinate along the field line changes sign $s \rightarrow -s$. This additionally leaves the fourth term on the left-hand side invariant. However, the terms on the right-hand side are invariant only if $F_{\rm M}$ is even in the parallel velocity, i.e. the equilibrium does not have a net parallel flow (zero background rotation $\Omega = 0$), and the gradient in the parallel velocity is zero (no gradient in the background rotation $\nabla\Omega = 0$). Turning to the drift due to the magnetic field inhomogeneity: in the local limit the drift depends only on the coordinate along the field line

$$\boldsymbol{v}_D \cdot \nabla = D^y(s) \frac{\partial}{\partial y} + D^r(s) \frac{\partial}{\partial r}. \tag{5}$$

The equation is invariant if $D^y(s) = D^y(-s)$ which is true for a magnetic equilibrium that is up–down symmetric. However, even for an up–down symmetric equilibrium, the radial component of a vertical drift changes sign when going from the lower to the upper half of the equilibrium, i.e. $D^r(s) = -D^r(-s)$. The equation can be made invariant only through the transformation $r \rightarrow -r$. The latter transformation then requires (through the third term in equation (4)) that the background $E \times B$ velocity is even in r and, hence, no background $E \times B$ shearing is allowed. Furthermore, the Maxwellian $F_{\rm M}$ must be even in r, which is satisfied in the local limit. With these transformations, the linear equation is invariant [5], but the nonlinear term still changes sign

$$\boldsymbol{v}_E \cdot \nabla = \frac{\partial \langle\phi\rangle}{\partial r} \frac{\partial}{\partial y} - \frac{\partial \langle\phi\rangle}{\partial y} \frac{\partial}{\partial r}. \tag{6}$$

The transformation [38] $f \rightarrow -f$ and $\phi \rightarrow -\phi$ changes the sign of all of the linear terms, but leaves the nonlinear term unchanged. Multiplying the original equation with -1 and using the transformations discussed above, the gyro-kinetic equation is invariant, while the toroidal momentum flux changes sign. The procedure has been outlined here for the electro-static collisionless case without considering the field equations. The extension to the electro-magnetic case with collisions as well as the analysis of the field equations is, however, straightforward. The transformations derived above are still valid and the procedure yields only the new transformation rules $A_\parallel \rightarrow A_\parallel$ and $\delta B_\parallel \rightarrow -\delta B_\parallel$. We note here that also for the field equations the symmetry holds only to lowest order in the normalized Larmor radius.

In conclusion the nonlinear electro-magnetic gyro-kinetic δf equation including the effect of collisions is invariant under the transformations

$$\begin{aligned}
&v_\parallel \rightarrow -v_\parallel \quad s \rightarrow -s \quad r \rightarrow -r \\
&f \rightarrow -f \quad \phi \rightarrow -\phi \quad A_\parallel \rightarrow A_\parallel \quad \delta B_\parallel \rightarrow -\delta B_\parallel
\end{aligned} \tag{7}$$

provided five conditions are satisfied:

- In the gyro-kinetic equation only the lowest order (in $\rho_* = \rho/R$) terms are kept. Note that in this limit the parallel velocity nonlinearity does not appear. Also in this limit the turbulence is homogeneous in the plane perpendicular to the magnetic field.
- There is no background toroidal rotation ($\Omega = 0$).
- There is no background parallel velocity gradient ($\nabla\Omega = 0$).
- There is no background $E \times B$ shearing (this was not considered in [5], but evident from the work of [39]).
- The equilibrium is up–down symmetric.

If $[f(r, y, s, v_\parallel, \mu, t), \phi(r, y, s), A_\parallel(r, y, s), \delta B_\parallel(r, y, s)]$ is a solution of the gyro-kinetic equation, then $[-f(-r, y, -s, -v_\parallel, \mu, t), -\phi(-r, y, -s), A_\parallel(-r, y, -s), -\delta B_\parallel(-r, y, -s)]$ satisfies the equation as well. Linearly both solutions have the same growth rate, and nonlinearly they occur with equal probability. The toroidal momentum flux for these two solutions, however, has the opposite sign. This is obvious for the approximation given in equation (3), but the result is more general. It can readily be verified that the transformation flips the sign of all momentum contributions in equation (2).

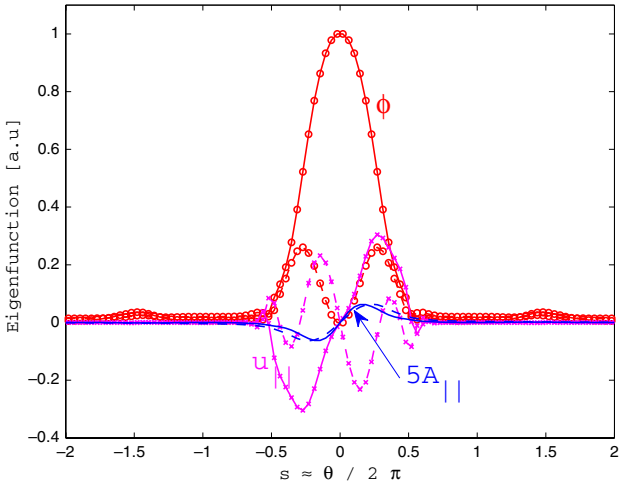

Figure 1. Eigenfunction normalized such that $\mathrm{Re}[\phi(s=0)]=1$, as a function of the coordinate along the field $s \approx \theta/2\pi$. Shown are the perturbed potential ϕ (circles), the parallel velocity perturbation $u_\parallel = \int v_\parallel f \, \mathrm{d}^3\boldsymbol{v}/n_\mathrm{i}$ of the ions (crosses), and the perturbed vector potential $A_\parallel$ times 5 (without symbols). For the normalization of $u_\parallel$ and $A_\parallel$ see [41]. The full lines are the real, while the dotted lines are the imaginary part.

In linear theory, for the most unstable mode, the symmetry described above can be directly observed in the mode structure, i.e. $f(r, y, s, v_\parallel, \mu, t) = f(-r, y, -s, -v_\parallel, \mu, t)$ as shown in figure 1 obtained with GKW [40, 41] for an electro-magnetic case based on the GA standard case ($R/L_{T\mathrm{i}} = R/L_{T\mathrm{e}} = 9$, $R/L_\mathrm{N} = 3$, $T_\mathrm{e}/T_\mathrm{i} = 1$, $q = 2$, $\hat{s} = 1$, $\epsilon = r/R = 0.166$, collisionless with kinetic electrons, deuterium mass ratio, $k_y\rho_\mathrm{i} = 0.42$ ($k_y\rho_\mathrm{s} = 0.3$ with $\rho_\mathrm{s} = c_\mathrm{s}/\omega_\mathrm{ci}$, $c_\mathrm{s} = \sqrt{T_\mathrm{e}/m_\mathrm{i}}$, and $\omega_\mathrm{ci} = eB/m_\mathrm{i}$) and $\beta_\mathrm{e} = 0.3\%$). The potential is then symmetric in the mid-plane ($s = 0$) while the parallel velocity fluctuations as well as the perturbed parallel vector potential are anti-symmetric. This yields zero net parallel momentum transport when integrating over the flux surface, with the flux generated at the top half of the torus being compensated by the bottom half. The nature of the symmetry transformation is perhaps somewhat puzzling. The transformation is not an expression of toroidal symmetry, but rather deals with the parity of the mode (up–down/in–out). As is clear from the linear mode example, the flux does not vanish locally, but rather is compensated between the lower and upper half of the surface, with the flux surface average yielding a zero net result.

3. Momentum flux contributions

The symmetry property is a powerful tool in interpreting the momentum flux. First, it follows directly that there are no off-diagonal contributions to the angular momentum flux driven by the density and temperature gradients. Note that this does not mean that the density and temperature gradients do not influence the momentum flux. They do since they form the main drive of the turbulence. It means that density and temperature gradients alone do not lead to a momentum flux since these gradients do not result in a breaking of the symmetry in the local limit. Second, it allows for a systematic identification of the mechanisms that can drive momentum transport. All must be connected with violating one or more of the constraints mentioned in the previous section. Indeed, it has been found that a violation of each of the conditions given above can generate a momentum flux, although it must be stressed that the breaking of symmetry is a necessary but not a sufficient condition. If the terms that break the symmetry are sufficiently small, a perturbation theory can be applied to arrive at an expression for the angular momentum flux which is linear in the symmetry breaking mechanisms. This is illustrated for the example of the $E \times B$ shearing below.

First assume that the solution (f_0, ϕ_0) of the equation without any symmetry breaking terms is known

$$\begin{aligned}\frac{\partial f_0}{\partial t} + v_\parallel \frac{\partial f_0}{\partial s} + (\boldsymbol{v}_D + \boldsymbol{v}_{E0})\cdot\nabla f_0 - \mu\frac{\partial B}{\partial s}\frac{\partial f_0}{\partial v_\parallel} \\ = -\frac{1}{B}\frac{\partial\langle\phi_0\rangle}{\partial y}\left[\frac{1}{L_n} + \left(\frac{mv^2}{2T} - \frac{3}{2}\right)\frac{1}{L_T}\right]F_\mathrm{M} \\ - \left(v_\parallel\frac{\partial\langle\phi_0\rangle}{\partial s} + \boldsymbol{v}_D\cdot\nabla\langle\phi_0\rangle\right)\frac{Ze}{T}F_\mathrm{M}. \end{aligned} \tag{8}$$

Second assume a small background $E \times B$ shear ($\boldsymbol{v}_{EB}$), such that equation (4) can be linearized to obtain

$$\begin{aligned}\frac{\partial f_1}{\partial t} + v_\parallel \frac{\partial f_1}{\partial s} + (\boldsymbol{v}_D + \boldsymbol{v}_{E0})\cdot\nabla f_1 + \boldsymbol{v}_{E1}\cdot\nabla f_0 - \mu\frac{\partial B}{\partial s}\frac{\partial f_1}{\partial v_\parallel} \\ + \frac{1}{B}\frac{\partial\langle\phi_1\rangle}{\partial y}\left[\frac{1}{L_n} + \left(\frac{mv^2}{2T} - \frac{3}{2}\right)\frac{1}{L_T}\right]F_\mathrm{M} \\ + \left(v_\parallel\frac{\partial\langle\phi_1\rangle}{\partial s} + \boldsymbol{v}_D\cdot\nabla\langle\phi_1\rangle\right)\frac{Ze}{T}F_\mathrm{M} = -\boldsymbol{v}_{EB}\cdot\nabla f_0 \\ = -\gamma_E\frac{\partial f_0}{\partial y}r, \end{aligned} \tag{9}$$

where $\gamma_E = \mathrm{d}v_{EB}/\mathrm{d}r$ is the $E\times B$ shearing rate. The left-hand side of this equation is linear in (f_1, ϕ_1) (with the potential ϕ_1 obtained from f_1 through the Poisson equation). The general solution of this equation cannot be expected to satisfy $f_1 \ll f_0$ since it contains the same linear instabilities when compared with the original equation. The equation above, however, is an inhomogeneous differential equation, and a bounded particular solution can be found since for long time intervals

$$\left\langle \gamma_E\frac{\partial f_0}{\partial y}r\right\rangle_\mathrm{time} \to 0. \tag{10}$$

The particular solution is linear in γ_E and so is its contribution to the flux

$$\begin{aligned}\Gamma^r_{\parallel,\mathrm{sp}} &= -\frac{RB_\mathrm{t}}{B}\int \mathrm{d}^3\boldsymbol{v}\,\frac{m_\mathrm{sp}v_\parallel}{B}\left(\frac{\partial\langle\phi_1\rangle}{\partial y}f_{0,\mathrm{sp}} + \frac{\partial\langle\phi_0\rangle}{\partial y}f_{1,\mathrm{sp}}\right) \\ &= m_\mathrm{sp}n_\mathrm{sp}\chi_{\varphi\perp}R_a\gamma_E, \end{aligned} \tag{11}$$

where R_a is the major radius of the magnetic axis. The linearization is valid when

$$\boldsymbol{v}_{E0}\cdot\nabla f_0 \gg \boldsymbol{v}_{EB}\cdot\nabla f_0 \quad\to\quad k_\perp\phi_0/B \gg v_{EB}. \tag{12}$$

The shearing rate has a global profile, while the fluctuating $E\times B$ velocity varies over the size of the eddy. Applying the criteria above to the change in $E\times B$ velocity over the eddy size yields

$$|\nabla v_{E0}| = k_\perp^2\phi_0/B \gg |\nabla v_{EB}| = \gamma_E \quad\to\quad \gamma_E \ll (k_\perp\rho)^2\frac{v_\mathrm{th}}{R}, \tag{13}$$

where in the latter step $\phi_0 = \mathcal{O}(\rho_* T/e)$ has been used. Since the growth rates of the instabilities are often in the range $(k_\perp \rho) v_{\rm th}/R$, the criterion derived above can also be roughly read as $\gamma_E \ll \gamma$, i.e. the momentum flux is linear in γ_E as long as no strong $E \times B$ shear stabilization of turbulence occurs [42].

If all the symmetry breaking terms can be ordered small, one obtains a momentum flux that is linear in the symmetry breaking terms

$$\Gamma_\varphi^{\rm N} = \chi_{\varphi\parallel}^{\rm N} u' + (V_\varphi^{\rm N} + \Gamma^{\rm N}) u + \chi_{\varphi\perp}^{\rm N} \gamma_E^{\rm N} + C_{FS}^{\rm N} + \rho_* C_*^{\rm N}. \quad (14)$$

Here, the superscript N denotes a normalized quantity

$$\Gamma_\varphi^{\rm N} = \frac{\Gamma_\varphi}{\sum_{\rm sp} m_{\rm sp} n_{\rm sp} R_a \rho_*^2 v_{\rm thi}^2} \qquad \Gamma^{\rm N} = \frac{\sum_{\rm sp} m_{\rm sp} \Gamma_{\rm sp}}{\sum_{\rm sp} m_{\rm sp} n_{\rm sp} \rho_*^2 v_{\rm thi}}$$

$$C_{FS}^{\rm N} + \rho_* C_*^{\rm N} = \frac{\Gamma_{\varphi,FS} + \Gamma_{\varphi *}}{\sum_{\rm sp} m_{\rm sp} n_{\rm sp} R_a \rho_*^2 v_{\rm thi}^2}$$

$$\chi_{\varphi\parallel}^{\rm N} = \frac{\sum_{\rm sp} m_{\rm sp} n_{\rm sp} \chi_{\varphi\parallel}^{\rm sp}}{\sum_{\rm sp} m_{\rm sp} n_{\rm sp} \rho_{\rm i}^2 v_{\rm thi}/R_a}$$

$$V_\varphi^{\rm N} = \frac{\sum_{\rm sp} m_{\rm sp} n_{\rm sp} R_a V_\varphi^{\rm sp}}{\sum_{\rm sp} m_{\rm sp} n_{\rm sp} \rho_{\rm i}^2 v_{\rm thi}/R_a}$$

$$\chi_{\varphi\perp}^{\rm N} = \frac{\sum_{\rm sp} m_{\rm sp} n_{\rm sp} \chi_{\varphi\perp}^{\rm sp}}{\sum_{\rm sp} m_{\rm sp} n_{\rm sp} \rho_{\rm i}^2 v_{\rm thi}/R_a}$$

$$u = \frac{R_a \Omega}{v_{\rm thi}} \qquad u' = \frac{R_a^2 \nabla \Omega}{v_{\rm thi}} \qquad \gamma_E^{\rm N} = \frac{R_a}{v_{\rm thi}} \frac{{\rm d}v_{EB}}{{\rm d}r}, \quad (15)$$

Γ is the mass weighted particle flux, and $v_{\rm thi} = \sqrt{2T_{\rm i}/m_{\rm i}}$ is the thermal velocity of the ions. The toroidal momentum flux consists of various contributions: the first term is the diagonal contribution (i.e. proportional to u'), the second is the Coriolis pinch (proportional to u), the third is due to the $E \times B$ shearing (proportional to γ_E), the fourth is the effect of an up–down asymmetric equilibrium, and the fifth is the collection of all effects that require a higher order ρ_* term in the gyro-kinetic equation. The latter term is naturally ρ_* smaller compared with the first four, which is explicitly denoted by taking ρ_* out of the coefficient. Note that the diagonal part is defined with respect to the gradient in Ω, a flux function to lowest order. The sign of the diagonal part may be confusing, but is simply due to the minus sign in the definition of the gradient, i.e. $u' = -R_a^2 \nabla \Omega / v_{\rm thi}$, a choice that results in a positive u' for the usually peaked rotation profiles. Below, unless explicitly denoted otherwise, the quantities are normalized and the superscript N will be dropped.

To determine the limit of applicability of the linear form of the momentum flux given above, one can compare the symmetry breaking terms with the corresponding terms in the gyro-kinetic equation, as has been shown for the $E \times B$ velocity above. This yields

$$u' \ll R/L_T \qquad u \ll 0.5 \qquad \gamma_E \ll (k_\perp \rho)^2 v_{\rm th}/R$$
$$\gamma_E \ll \gamma_{\rm max}. \quad (16)$$

The up–down asymmetry term is, however, somewhat more difficult to quantify. In principle one can write the geometric quantities as the sum of a symmetric and a anti-symmetric part. If the latter is small compared with the former one can treat it as a perturbation. This, however, does not directly produce a single dimensionless quantity which can be used to estimate under what conditions the flux is linear. For the finite ρ_* terms the linearization should always apply since $\rho_* \ll 1$. When the perturbation theory applies, all coefficients $(\chi_{\varphi\parallel}, V_\varphi, \chi_{\varphi\perp}, C_{FS}, C_*)$ are independent of the symmetry breaking terms $(u', u, \gamma_E, ..)$. Note though that the coefficients are of course strongly nonlinear functions in the gradients that drive the turbulence.

The inequalities of equation (16) are generally met for the standard H-mode (with typically $u' \approx 1$, $u \approx 0.2$, $\gamma_E < \gamma$), but might fail for transport barriers or strongly rotating plasmas. Experiments on ASDEX Upgrade [5] satisfy $u' < R/L_T$ even for transport barriers, but the condition $\gamma_E < \gamma_{\rm max}$ is not satisfied since the $E \times B$ shear leads to a substantial stabilization of the turbulence. Indeed, it has been shown that the momentum flux due to the $E \times B$ shear shows a relatively strong nonlinear behaviour [43, 44] that will be discussed further below. Most tokamak plasmas satisfy $u < 0.5$, but due to their compact nature spherical tokamaks can rotate at velocities $u \approx 1$. In the latter case not only the Coriolis, but also the centrifugal force connected with the plasma rotation must be considered. The effects of the centrifugal force are expected to be small [45], but have so far not been systematically studied.

The $E \times B$ shearing rate is due to the toroidal velocity shear as well as the pressure gradient and poloidal rotation shear. Using the radial force balance and the neo-classical expression for the poloidal rotation $V_\theta = \alpha \nabla T/eB$, where α is of order unity and depends on the collisionality regime, one arrives at

$$\gamma_E = \frac{B_{\rm p}}{B_{\rm t}} u' - \frac{1}{2} \rho_* \left[\frac{R^2}{n} \frac{{\rm d}^2 n}{{\rm d}r^2} + (1-\alpha) \frac{R^2}{T} \frac{{\rm d}^2 T}{{\rm d}r^2} + 2 \frac{R^2}{nT} \frac{{\rm d}n}{{\rm d}r} \frac{{\rm d}T}{{\rm d}r} \right], \quad (17)$$

where derivatives of the magnetic components have been neglected against the profile derivatives. Through the dependence of γ_E on u' the momentum flux due to the $E \times B$ shearing acts as a correction to the diagonal component of the momentum flux. The second term on the right-hand side is independent of the toroidal rotation or its gradient, and is one order smaller in ρ_*. Momentum flux terms that are independent of the velocity or its gradient are referred to as residual stress.

One might be tempted to consider the ρ_* terms in the toroidal momentum equation small under all circumstances. This is not necessarily justified. The second term on the right-hand side of equation (17) for γ_E is proportional to the second derivative of the density and temperature profiles. Adopting $2(R/L_T)^2$, as a simple estimate for the term in the square brackets, one recognizes that the second term on the right-hand side of equation (17) is roughly $40\rho_*$ ($R/L_T \approx 6$) in the core and increases to values larger than $1000\rho_*$ ($R/L_T > 30$) in the plasma edge. While the $E \times B$ shearing can therefore be expected to be relatively small in the core under most conditions, this statement is certainly not true for the edge, where it could dominate the momentum flux. A more accurate criterion for the importance of finite ρ_* terms can be derived by comparing the momentum flux due to $E \times B$ shearing with the Coriolis pinch effect. Assuming $V_\varphi \approx \chi_{\varphi\perp}$, which is roughly satisfied (see below), one arrives at the following criterion:

$$u > \rho_* (R/L_T)^2 \quad (18)$$

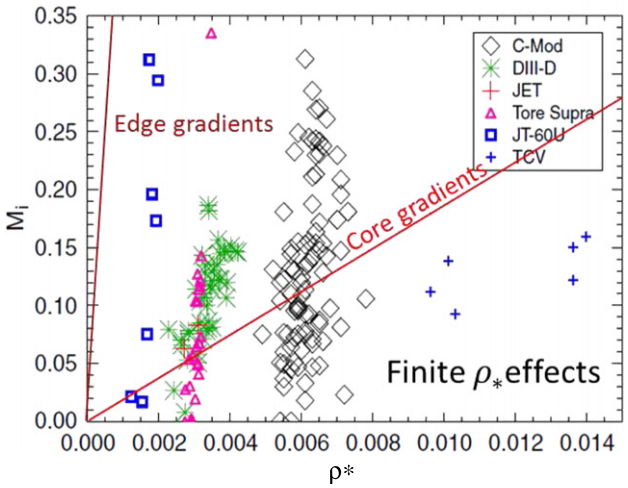

Figure 2. Adapted from [29]. Mach number of the intrinsic rotation observed in various experiments as a function of ρ_*. The lines indicate the result of equation (18) for typical values of the core ($R/L_T = 6$) and edge ($R/L_T = 30$) gradients. Note that both ρ_* as well as the Mach number are defined differently in this figure compared with the main text: $\rho_{*F} = \rho_*/\sqrt{(2)}$. $M_i = \sqrt{2}u$, where the subscript F refers to the value of the figure.

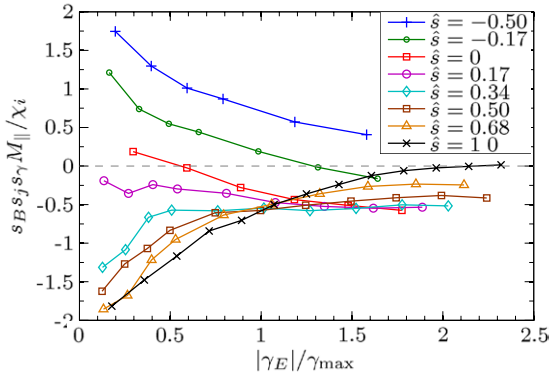

Figure 3. Reprinted with permission from [44]. Copyright 2009, American Institute of Physics. Ratio of the transport coefficients $\chi_{\varphi\perp}/\chi_i$ as a function of the shearing rate normalized to the maximum growth rate for various values of the magnetic shear. The quantities s_B, s_J, and s_γ represent the sign of the magnetic field, current and shearing rate. Furthermore $M_\parallel = \chi_{\varphi\perp}$. Simulation parameters are those of the GA standard case with adiabatic electrons. Further details on the computations can be found in [44].

which, when satisfied, implies that the finite ρ_* effects can be neglected.

The condition under which the finite ρ_* effects can be neglected under experimental relevant conditions is clarified in figure 2 from [29], which shows the Mach number of the intrinsic rotation as a function of ρ_* for various experiments (note that both the definition of the Mach number as well as that of ρ_* are different in [29] compared with the definitions adopted here). In this diagram lines are drawn above which the $E \times B$ shear momentum flux due to finite ρ_* effects can be neglected for typical core and edge gradients. None of the experimental points lie above the line for the edge gradients and, consequently, the finite ρ_* effects are never negligible in the edge. At small ρ_* the experiments do lie above the line for typical core gradients, such that only the toroidal velocity shear must be kept in the evaluation of the $E \times B$ shear. This does not apply to all experiments. All data from TCV, for instance, lie in the domain for which finite ρ_* effects are important even in the core of the plasma.

For larger experiments, and especially reactor experiments such as ITER, the finite ρ_* effects in the core can be neglected leading to a momentum flux of the form

$$\Gamma_\varphi = \left(\chi_{\varphi\parallel} + \frac{B_p}{B_t}\chi_{\varphi\perp}\right)u' + V_\varphi u + \mathcal{O}[\rho_*\chi_{\varphi\perp}(R/L_T)^2], \quad (19)$$

i.e. the momentum flux is in the form of a diffusion and a pinch. In the form above we have also neglected the effect of the up–down asymmetry, since it has been found (see below) that the effect decreases rapidly from edge to core.

The momentum flux given in equation (19) is proportional to the rotation or its gradient. For zero toroidal velocity, the momentum flux is zero, and no spin up of the plasma will occur. A seed rotation which allows the pinch to transport the momentum inwards, generating a peaked rotation profile, is therefore necessary. For a large tokamak this seed rotation then is largely generated at the edge of the plasma and is due to the up–down asymmetry, boundary conditions (i.e. flows in the scrape-off layer [46, 47]) or finite ρ_* effects. The shape of the profile in the core is determined by the diffusion and pinch coefficients with the magnitude of the rotation velocity at the centre being proportional to the seed rotation. The seed rotation, therefore, plays an important role in the determination of the rotation value, and our limited understanding of the plasma edge at present prevents a prediction of the magnitude of the rotation in ITER.

4. Contributions to the momentum flux

4.1. $E \times B$ shearing

Background $E \times B$ shearing breaks the $r \to -r$ symmetry and can induce a flux of toroidal momentum [39, 43, 44, 48, 49]. The symmetry breaking also induces an asymmetric parallel mode structure. The process can, in simple terms, be understood as follows. The shearing rotates the eddy structures increasing the perpendicular wave number which leads to stabilization of the mode. However, the magnetic field also has a shear and the mode can partly 'escape' the effect of the $E \times B$ shear by moving along the field while growing such that the magnetic shear partly undoes the effect of the $E \times B$ shear. It thereby shifts the position of maximum wave amplitude away from the low-field side leading to an asymmetry in the parallel mode structure. Indeed the momentum flux changes sign with the sign reversal of the magnetic shear [44, 48, 49], although the result is not exact, i.e. symmetry breaking persists at zero magnetic shear.

The effect of $E \times B$ shearing has been studied through nonlinear gyro-kinetic simulations. The ratio of the coefficients $\chi_{\varphi\perp}/\chi_i$ is shown in figure 3 (from [44]) as a function of the $E \times B$ shearing rate normalized to the maximum growth rate of the modes, for various values of the magnetic shear. For small shearing rates $\gamma_E \ll \gamma_{\max}$ the ratio $\chi_{\varphi\perp}/\chi_i$ is independent of γ_E, but at larger values the ratio decreases with the $E \times B$ shearing rate. This is not due to the familiar $E \times B$ shear stabilization, since the ratio of the transport

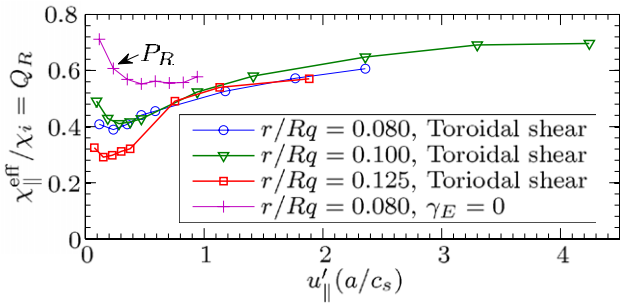

Figure 4. Reprinted with permission from [44]. Copyright 2009, American Institute of Physics. Prandtl number χ_φ/χ_i as a function of the toroidal velocity gradient $u'_\parallel = \sqrt{2}au'/R \approx 0.47u'$ for various values of $B_p/B = r/qR$. Parameters are those of the GA standard case with adiabatic electrons. The curves indicated with 'toroidal shear' have an $E \times B$ shear that is consistent with the gradient in the toroidal rotation u'.

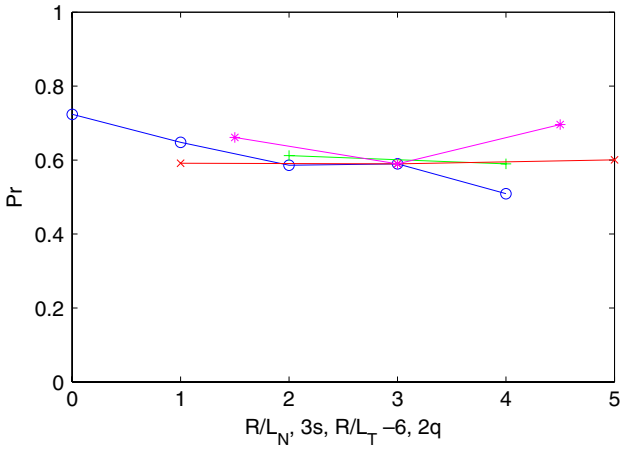

Figure 5. Prandtl number $Pr = (\chi_{\varphi\parallel} + B_p\chi_{\varphi\perp}/B_t)/\chi_i$ as a function of density gradient (circles), the magnetic shear (stars), the temperature gradient (x) and safety factor (+). To plot the curves on one graph the x-axis for each of the scans is modified. It represents R/L_N, $3\hat{s}$, $R/L_T - 6$, and $2q$, respectively.

coefficients is insensitive to the turbulence level. The result of figure 3 rather shows that momentum transport due to $E \times B$ shearing becomes less efficient when background $E \times B$ shearing strongly stabilizes the transport. This nonlinear effect might complicate the interpretation of the edge of H-mode experiments where $E \times B$ shearing is strong. For $\gamma_E \approx \gamma_{\max}$, the ratio $\chi_{\varphi\perp}/\chi_i$, furthermore becomes a function of u' [44] and it appears that cases of strong $E \times B$ shearing require nonlinear simulations to assess the momentum flux.

4.2. The diagonal contribution

A finite radial gradient in the angular frequency leads to a diagonal (diffusive) contribution. Early work based on fluid models already established a strong coupling between ion heat and momentum transport [18]. This coupling is expressed in the dimensionless Prandtl number (Pr), which is the ratio of the momentum and ion heat diffusivities $Pr = \chi_\varphi/\chi_i$. The Prandtl number has more recently been assessed through linear [5, 50, 51], and nonlinear gyro-kinetic simulations using adiabatic electrons [52, 53] as well as with full electron dynamics [43, 54–56] confirming a Prandtl number of order unity. The diagonal contribution is due to both the parallel velocity shear as well as the $E \times B$ shear connected with the gradient in the toroidal rotation, i.e. $\chi_\varphi = \chi_{\varphi\parallel} + B_p\chi_{\varphi\perp}/B_t$. Due to the very different nature of the parallel and perpendicular dynamics, it can, however, be useful to calculate the contributions separately. Furthermore, due to smallness of the ratio B_p/B_t, the contribution of the parallel velocity transport is expected to dominate. For these reasons several (but not all) of the above mentioned studies calculate $\chi_{\varphi\parallel}$ instead of χ_φ.

Figure 4 shows the momentum diffusivity ($\chi_\varphi = \chi_{\varphi\parallel} + B_p\chi_{\varphi\perp}/B$) normalized with the ion heat conductivity (χ_i) as a function of u'. The different curves are for different values of $B_p/B = r/qR$, resulting in a different contribution of $\chi_{\varphi\perp}$ to χ_φ. For a sufficiently positive magnetic shear, the $E \times B$ shearing contribution always reduces the momentum diffusivity independent of the sign of the magnetic field or plasma current. The decrease can be quite substantial with values as low as $\chi_\varphi/\chi_i = 0.3$ being reached. (The presented simulations use the adiabatic electron approximation. Kinetic electrons in general give a somewhat larger value.) At larger values of u' and, consequently, larger values of γ_E, the reduced efficiency of the $E \times B$ shear driven momentum transport makes that the various curves approach each other.

Figure 5 shows the Prandtl number $Pr = (\chi_{\varphi\parallel} + B_p\chi_{\varphi\perp}/B_t)/\chi_i$ as a function of various plasma parameters. In the various scans only one of the parameters has been varied while keeping all others fixed to the GA standard case ($R/L_{Ti} = R/L_{Te} = 9$, $R/L_N = 3$, $T_e/T_i = 1$, $\hat{s} = 1$, $q = 2$, $\epsilon = 0.16$, electro-static collisionless with kinetic electrons and Deuterium mass ratio). To calculate the diagonal part, the background plasma rotation is chosen to be (locally) zero ($u = 0$) with a finite gradient $u' = 1$. Simulations have been performed assuming a circular geometry, keeping finite inverse aspect ratio effects (different from the common $\hat{s} - \alpha$ geometry that treats the inverse aspect ratio to lowest order only). All simulations use 21 toroidal modes (only positive are counted) with a maximum bi-normal wave vector $k_y\rho_i = 1.414$ ($k_y\rho_s = 1$), and 141 radial modes (both signs) with a maximum $k_r\rho_i = 5.2$ ($k_r\rho_s = 3.6$). The transport coefficients are obtained by averaging over a time interval $t = (50 - 450)R/v_{thi}$. Further details of the simulations will be discussed in [56]. From the figure it is clear that the Prandtl number does not vary strongly with the plasma parameters.

The values of the Prandtl number reported in the literature cover a range 0.24–1.2. This is in itself not entirely surprising since the values have been obtained for different plasma parameters, and the Prandtl number is not a universal constant. Nevertheless, the result of the flux tube simulations yield a relatively weak dependence on plasma parameters, and therefore suggest that differences in the definition of the Prandtl number could play a role. As already mentioned some of the simulations evaluate only the parallel contribution $\chi_{\varphi\parallel}$, and some use the adiabatic electron approximation. Furthermore, in global simulations, finite ρ_* effects can generate an additional momentum flux such that an effective Prandtl number is obtained. These include large scale long lived zonal flows which have been observed to influence the momentum flux [55]. Differences can furthermore occur if one defines the diagonal contribution with respect to the

gradient in the toroidal velocity, rather than the gradient in the angular rotation frequency Ω. And finally, we note that the GA standard case has a temperature gradient well above the threshold of the instability. Some simulations, and indeed the experiment, have gradients close to the threshold. A more extended study is necessary to clarify these points.

4.3. The Coriolis pinch effect

The symmetry is also broken for a toroidally rotating plasma, leading to a momentum pinch [57, 58]. In the local limit, the effect can be elegantly derived by transforming to the reference frame that moves with the plasma [57]. We stress here that only in this section 4.3 we use the co-moving system. All other expressions presented in this paper are formulated in the laboratory frame. In the co-moving frame the plasma rotation is naturally zero, and enters the physics description only through the Coriolis and centrifugal forces. It is the Coriolis force ($\boldsymbol{F}_{\rm co}$) that is of main interest in the generation of momentum transport [45] and the centrifugal force will be neglected below. In a magnetized plasma this force generates a Coriolis drift velocity [57, 59]

$$\boldsymbol{F}_{\rm co} = 2mv_{\parallel}\boldsymbol{b}\times\boldsymbol{\Omega} \quad \rightarrow \quad \boldsymbol{v}_{\rm co} = \frac{2mv_{\parallel}}{ZeB}\boldsymbol{\Omega}_{\perp}. \tag{20}$$

The plasma rotation then enters the gyro-kinetic equation only through this additional drift

$$\frac{\partial f}{\partial t} + \frac{2mv_{\parallel}}{ZeB}\boldsymbol{\Omega}_{\perp}\cdot\nabla f + \cdots = \cdots - \frac{2mv_{\parallel}}{ZeB}\boldsymbol{\Omega}_{\perp}\cdot\nabla\langle\phi\rangle\frac{Ze}{T}F_{\rm M} \tag{21}$$

were the dots represent the terms given in equation (4). The Coriolis drift, like the drift due to the magnetic field inhomogeneity, enters the equation as a convection as well as through an acceleration of the particles due to the drift in the gradient of the perturbed potential. Taking the parallel velocity moment of equation (21) one obtains

$$mn\frac{\partial w}{\partial t} + \frac{2m\boldsymbol{\Omega}_{\perp}}{ZeB}\cdot\nabla p_{\parallel} + \cdots = \cdots - 2nm\boldsymbol{\Omega}_{\perp}\cdot\nabla\langle\phi\rangle/B, \tag{22}$$

where w is the perturbed velocity and $p_{\parallel}$ is the perturbed parallel pressure. The second term on the left-hand side, which can be written as $-2m\boldsymbol{v}_{d\parallel}\times\boldsymbol{\Omega}$ with $\boldsymbol{v}_{d\parallel} = \boldsymbol{b}\times\nabla p_{\parallel}/ZeB$, is the Coriolis force due to the perturbed diamagnetic velocity, while the term on the right-hand side ($-2nm\boldsymbol{\Omega}_{\perp}\cdot\nabla\langle\phi\rangle/B = 2mn\boldsymbol{v}_E\times\boldsymbol{\Omega}$) is the Coriolis force due to the perturbed $E\times B$ velocity. From equation (22) it can be seen that the parallel pressure perturbation, through the convection of the Coriolis drift, generates parallel velocity fluctuations. It is the Coriolis drift, which is linear in the parallel velocity, that generates the coupling between an even moment of the perturbed distribution (the pressure) and the velocity perturbation. The drifts due to the inhomogeneous magnetic field, which are proportional to the velocity squared, couple the even moments of the distribution (density, temperature), but not even with odd moments. The $E\times B$ transport of the parallel velocity fluctuations generated by the parallel pressure lead to a flux of parallel momentum. Furthermore, the acceleration of the particles due to the Coriolis drift in the gradient of the perturbed potential, represented by the term on the right-hand side of equation (22), generates parallel velocity fluctuations, and thus a flux of toroidal momentum also results through the action of this term. A closed analytic expression for the pinch can be derived for a low-field side ITG model with the adiabatic electron approximation [57, 60]:

$$\frac{V_{\varphi}}{\chi_{\varphi}} = \left(-2\frac{R}{L_{\rm N}} + 4 - \frac{4}{\tau}\right) + \left(-4 + \frac{R}{L_{\rm N}}\right) = -\frac{4}{\tau} - \frac{R}{L_{\rm N}}, \tag{23}$$

where τ is the electron to ion temperature ratio $\tau = T_{\rm e}/T_{\rm i}$. In the equation above the first term in the brackets is due to the convection, whereas the second term in the brackets is due to the acceleration. The Coriolis pinch is inwards and enhances the rotation profile peaking independent of the direction of the rotation.

The Coriolis pinch given in equation (23) is derived in the co-moving system. Indicating the laboratory system with the subscript L, the transformation

$$v_{\parallel L} = v_{\parallel} + \frac{RB_{\rm t}}{B}\Omega \qquad \boldsymbol{E}_L = \boldsymbol{E} + \boldsymbol{B}\times R^2\Omega\nabla\varphi, \tag{24}$$

where $\boldsymbol{E}$ is the electric field, can be used to transform the results from the co-moving to the laboratory frame. Using this relation in equation (2) one can derive for the electro-statics case (the electro-magnetic case is somewhat more involved and will be discussed elsewhere)

$$\Gamma_{\varphi L} = \Gamma_{\varphi} + \sum_{\rm sp}\left\{m_{\rm sp}\left(\frac{RB_{\rm t}}{B}\right)^2\Gamma_{\rm sp}\right\}\Omega, \tag{25}$$

where $\Gamma_{\rm s}$ is the radial particle flux of species sp

$$\Gamma_{\rm sp} = \int v_{Er} f_{\rm sp}\,{\rm d}^3\boldsymbol{v}. \tag{26}$$

The flux in the laboratory frame is therefore the same as that of the co-moving system with the exception of an additional contribution related with the particle flux. The interpretation of the latter term is that the particles carry with them the averaged toroidal momentum when they move radially. For this reason this contribution to the flux does not appear in the co-moving system where the averaged toroidal velocity is zero.

The Coriolis pinch derived in the co-moving system is therefore present also in the laboratory frame, although its connection to the Coriolis force is obviously less clear. The theory in the laboratory frame has been worked out in [58], where the two contributions mentioned above have been identified as thermoelectric and $E\times B$ compression. The theories of the co-moving and laboratory frame have been shown to be equivalent in [61].

The vector $\boldsymbol{\Omega}$ points in the direction of the symmetry axis. For a tokamak to order ϵ^2, where ϵ is the inverse aspect ratio,

$$\boldsymbol{\Omega}_{\perp} \approx \frac{\boldsymbol{B}\times\nabla B}{B^2}R\Omega \tag{27}$$

and

$$-2mn\boldsymbol{\Omega}_{\perp}\cdot\frac{\nabla\langle\phi\rangle}{B} = 2mn\left(\boldsymbol{v}_E\cdot\frac{\nabla B}{B}\right)R\Omega = -mnR\Omega\nabla\cdot\boldsymbol{v}_E \tag{28}$$

where in the last step a low beta plasma was assumed. Within the approximation of equation (27), the term on the right-hand side of equation (22), which represents the acceleration

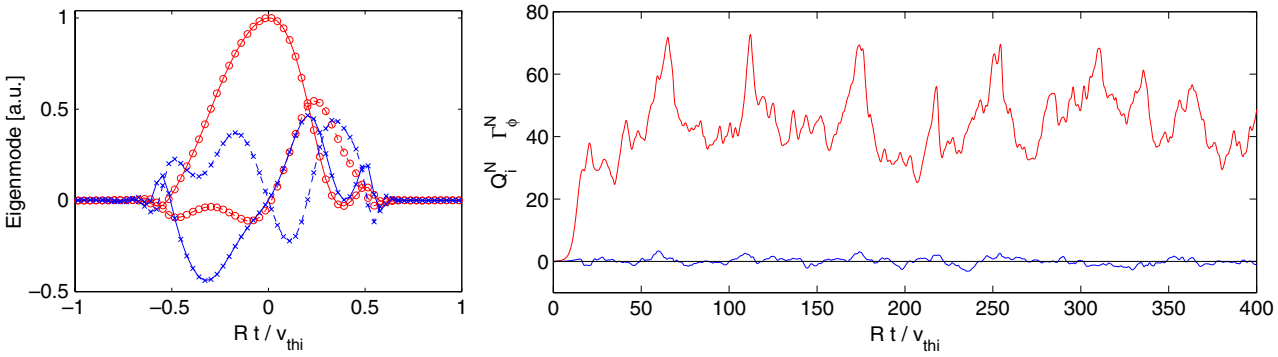

Figure 6. Left: the eigenfunction for the GA standard case with adiabatic electrons, $k_y\rho_i = 0.42$ $u' = 0$ and $u = 0.2$. Circles denote the perturbed potential while crosses represent the perturbed parallel velocity. Full lines represent the real, while dotted lines represent the imaginary part of the eigenfunction. Right: the ion heat (upper curve) and momentum flux (lower curve) as a function of time. The resolution is the same as for the simulations of the Prandtl number.

of the particles in the perturbed potential, is related to the compression of the perturbed $E \times B$ velocity. The latter formulation allows this effect (but not the one due to the convection) to be described within the framework of turbulence equipartition [62, 63].

The study of the Coriolis pinch effect has also revealed that the breaking of symmetry is a necessary, but not a sufficient condition [60]. Figure 6 shows the eigenfunction for the GA standard case with adiabatic electrons and $k_y\rho_i = 0.42$. The mode is clearly asymmetric in the low-field side mid-plane ($s = 0$). However, while a symmetric eigenfunction implies a zero momentum flux, an asymmetric eigenfunction does not necessarily mean a finite flux. Indeed, the momentum flux for this case is zero as shown in the right panel of figure 6. It can be shown [60] that the zero flux is generated by the combined effect of the Coriolis drift and a finite parallel wave vector. For the adiabatic electron case the most unstable mode has a parallel wave vector that exactly compensates the effect of the Coriolis drift, resulting in a zero toroidal momentum flux. A finite Coriolis pinch requires the description of kinetic electrons. In the presence of trapped electrons, the parallel mode structure is more restricted, preventing a complete cancellation between the Coriolis drift effect and the parallel wave vector of the eigenfunction. This leads to the counter intuitive result that the Coriolis pinch scales with the trapped electron fraction, i.e. $\sqrt{\epsilon}$, even though the electrons hardly carry any momentum. It also explains the poor performance of the fluid models in which kinetic electrons are not accounted for, like equation (23) above, which over-predicts the momentum pinch by roughly a factor 2 (for $\sqrt{\epsilon} = 0.4$). Finally, the sensitivity to the parallel wave vector explains the influence of electro-magnetic effects [64] which can strongly reduce the pinch close to the kinetic ballooning mode threshold.

Parameter dependences of the pinch from nonlinear gyro-kinetic simulations are shown in figure 7. Similar to the fluid model, the density gradient leads to an enhancement of the pinch. The Coriolis drift is in the vertical direction, and similar to the curvature drift, the mode needs to be localized on the outboard side of the surface for it to have an effect. A reduction in the Coriolis pinch is therefore observed when the mode is less localized. This explains the decrease of the pinch with the magnetic shear and the safety factor. It is to be noted that all

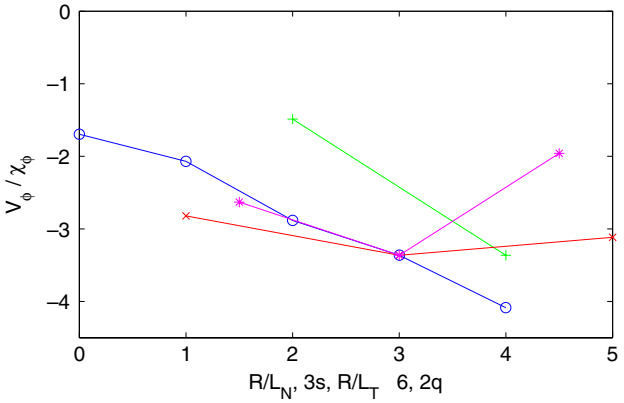

Figure 7. Pinch number V_φ/χ_φ for the GA standard case with kinetic electrons as a function of density gradient (circles), the magnetic shear (stars), the temperature gradient (x) and safety factor (+). To plot the curves on one graph the x-axis for each of the scans is modified. It represents R/L_N, $3\hat{s}$, $R/L_T - 6$, and $2q$, respectively. To determine the pinch the momentum flux is calculated for a finite background rotation $u = 0.2$, with zero rotation gradient $u' = 0$. The result of the runs from which the Prandtl number was determined (with $u' = 1$, $u = 0$) are then used to determine the ratio V_φ/χ_φ. The resolution, time window of averaging for the runs with $u = 0.2$ are the same as the runs from which the Prandtl number was determined.

the parameter dependences of the pinch (inverse aspect ratio, safety factor, magnetic shear) result in a small pinch in the inner core of the plasma. Finally, all of the examples in this section have dealt with the ITG. A pinch is, however, also observed for the trapped electron mode (TEM) [65].

4.4. The particle flux effect

The particle flux appears in the equation for the toroidal angular momentum conservation. Knowledge of the particle flux, which is well studied (see [66] and the references cited therein), directly allows for an evaluation of this contribution. Under stationary conditions with central NBI the particle flux is outwards and will reduce the total plasma angular momentum. Note that this mechanism, like the diagonal part and the Coriolis pinch, is not able to provide a seed rotation, since the flux of momentum is proportional to the background rotation.

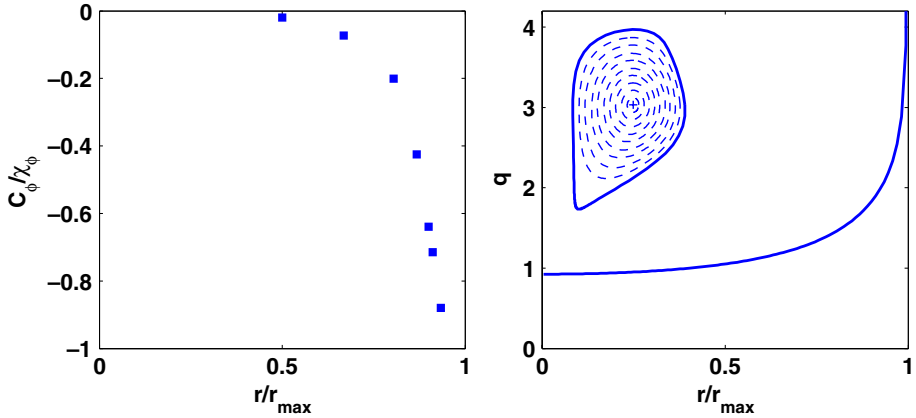

Figure 8. Reprinted with permission from [68]. Copyright 2009, American Institute of Physics. The left panel shows the ratio $C_{FS}/\chi_{\varphi\|}$ as a function of the normalized minor radius, for an equilibrium of TCV shown in the right panel. The right panel also shows the safety factor profile as a function of the normalized minor radius.

Due to the small particle fuelling, the particle flux and, consequently, the toroidal momentum flux associated with it will be relatively small under experimental relevant conditions. For NBI heated plasmas fuelling and heating are related. The total heat flux Q satisfies $Q = E\Gamma$, where E is the energy of the injected neutrals. This relation can be used to estimate the magnitude of the particle flux term compared with the diagonal contribution

$$\frac{m_\mathrm{i}R^2\Omega\Gamma}{m_\mathrm{i}n_\mathrm{i}\chi_\varphi R^2\nabla\Omega} = -\frac{\Gamma L_\Omega}{n_\mathrm{i}\chi_\varphi} \approx \frac{\Gamma L_\Omega T}{Q_\mathrm{i}L_T} = \frac{L_\Omega}{L_T}\frac{T}{E} \tag{29}$$

where $L_\Omega = -\nabla\Omega/\Omega$, and in the second step $\chi_\varphi \approx \chi_\mathrm{i}$ and $Q \approx Q_\mathrm{i} = -n_\mathrm{i}\chi_\mathrm{i}\nabla T$ have been used. Since $T/E \ll 1$ the particle flux term is usually only a few per cent compared to the diagonal contribution. In the case of wave heating the fuelling and, therefore, the particle flux effect will be smaller. Also for a reactor in which the plasma is largely heated by the fusion reactions, the particle fuelling relative to the heat flux will be smaller. In the edge of the plasma, however, neutrals can penetrate and the momentum flux connected with the particle flux could possibly be important.

4.5. Up-down asymmetric equilibrium

An up–down asymmetric equilibrium naturally breaks the symmetry along the magnetic field and a finite flux of toroidal momentum results [67–69]. In principle this symmetry breaking is connected with all geometry quantities, but studies have revealed that the asymmetry in the curvature operator and perpendicular wave vector generate 80% of the effect. A significant flux is only obtained if the extension of the mode along the field is large enough to 'feel' the asymmetry. Consequently, a maximum in the flux is often obtained for a relatively long wavelength $k_\perp\rho_\mathrm{s} \approx 0.15$, in contrast to the diagonal and pinch contribution. The complex interplay between the asymmetry of the equilibrium and the localization of the mode has so far prevented the development of a simple scaling formula to quantify, or even to determine the sign of, the momentum flux. For a given case, the momentum flux changes sign when the sign of the magnetic field or plasma current is changed, or when the equilibrium is flipped upside down. Unlike the other leading ρ_* effects, the up–down asymmetry generates a flux that is independent of the rotation or its gradient, i.e. it can provide a seed rotation. Its magnitude depends on the magnitude of the asymmetry which is found to strongly decrease with minor radius. Consequently, the effect is largest at the plasma edge as shown in figure 8. For the equilibrium, shown in the second panel of figure 8, the ratio of the coefficients $C_{FS}/\chi_{\varphi\|}$ reaches unity close to the edge. When integrated over the whole profile it predicts a core rotation of $u = 0.05$ (without considering any other mechanism that could further enhance the rotation of the core).

4.6. Higher order ρ_* terms

So far, the local limit or lowest order ρ_* approximation has been discussed. In higher order many different effects can break the symmetry. Or, perhaps better stated, there is no symmetry. The theory in this area is still under development and it appears that not all possible mechanisms have been explored. Known symmetry breaking mechanisms include a radial profile variation of the turbulent amplitude (or more correctly the turbulent wave quanta density) [70, 71], the parallel velocity nonlinearity (or polarization drift) [72, 73], $E \times B$ shearing connected with the pressure gradient contribution to the radial electric field [74], profile shearing [75, 76], and neo-classical effects [33].

The parallel velocity nonlinearity enters the gyro-kinetic equation in higher order in ρ_*.

$$\frac{\partial f}{\partial t} + \cdots - \frac{Ze}{m}\frac{\partial\langle\phi\rangle}{\partial s}\frac{\partial f}{\partial v_\|} - v_\| \frac{\boldsymbol{b}\times(\boldsymbol{b}\cdot\nabla)\boldsymbol{b}}{B}\cdot\nabla\langle\phi\rangle\frac{\partial f}{\partial v_\|} = \cdots. \tag{30}$$

For the symmetry to hold, all terms in the gyro-kinetic equation must change sign under the general transformation given in section 2. It is clear, however, that the velocity nonlinearity does not and, consequently, can be expected to drive a toroidal momentum flux. It has been shown [72] that the velocity nonlinearity can generate a momentum flux comparable in magnitude to the $E \times B$ shearing connected with the pressure gradient contribution.

When the local limit approximation is relaxed, the change in the density and temperature gradients over the simulation

domain leads to symmetry breaking [52]. A study of the global structure of the toroidal ITG mode reveals that when the mode frequency is radially sheared, the most unstable mode is tilted poloidally [78]. As for the case of $E \times B$ shearing, this poloidal tilt implies parallel symmetry breaking and momentum transport. The effect of profile shearing on momentum transport has been studied in the linear regime with the global gyro-kinetic code GT5D [79] as well as nonlinearly with GYRO simulations [76, 80]. The resulting momentum flux can be large $C_*/\chi_\phi \approx 1$ for $1/\rho_* = 150$, and changes sign at the ITG/TEM transition [75].

An interesting new development is the coupling of turbulence and the neo-classical equilibrium [33]. The neo-classical correction to the equilibrium distribution function is of order $(B/B_\mathrm{p})\rho_*(R/L_\mathrm{N})$ and, therefore, need not be kept in the lowest order ρ_* description. In next order it, however, must be included and since the neo-classical equilibrium contains plasma flows along the magnetic field, it breaks the symmetry and can be expected to lead to a radial momentum flux. This flux is expected to be larger by a factor $B/B_\mathrm{p} \approx 10$ compared with the turbulent induced fluxes and would then provide the dominant contribution to the finite ρ_* momentum flux. An analytic treatment has shown [33] that in order to calculate this momentum flux one needs to solve only the lowest order turbulence equation, i.e. the equation of the local limit, with the background distribution modified to include the neo-classical equilibrium.

For many finite ρ_* effects, an accurate assessment of the magnitude of the fluxes through numerical simulations is still lacking. Such simulations are necessary to ultimately decide which of the effects is dominant under what conditions.

5. Experimental observations

A detailed review of all experimental observations is beyond the scope of this paper. Here, we mostly highlight those experiments that give direct input to the theory and modelling.

The toroidal angular momentum transport is observed to be anomalous [81, 82]. Rotation profiles exhibit a non-stiff behaviour [17] and are strongly affected by the torque on the plasma, when present. The intrinsic rotation, i.e. the rotation the plasma develops without external momentum input, shows a rather complex behaviour in L-mode. The rotation direction is mostly observed to be in the counter current direction [83, 84], but is sensitive to the details of the geometry. Furthermore, at higher density a sudden transition to a different rotation profile is observed for a minimal change in density [85, 86]. In contrast the rotation in H-mode is mostly co-current and scales roughly with the plasma stored energy over the plasma current [29, 87]. The direction of the rotation (co or counter current) is difficult to predict theoretically. All lowest order ρ_* mechanisms, with the exception of the up–down asymmetry, do not have a preferred direction. The up–down asymmetry can lead to both co- as well as counter-current rotation, depending on the instability and details of the geometry. In the edge, finite ρ_* effects will play an important role and likely determine the direction of rotation. Our still limited understanding of the latter mechanisms prevents a definite answer on the question of the direction of intrinsic rotation.

The residual stress can be directly observed only for zero toroidal rotation velocity. On DIII-D experiments have been performed in which, through the combined use of co- and counter-beams, a nearly zero toroidal rotation has been generated over the entire plasma radius [88, 89]. A finite torque on the plasma is necessary to obtain this zero rotation state, a clear proof of the existence of a residual stress. The net torque needed to obtain the zero rotation state is significant, roughly corresponding to the torque of one beam box on DIII-D [88]. The radial profile has been determined recently through experiments in which the rotation velocity as a function of time goes through zero [90]. These experiments show that the residual stress is dominantly located at the plasma edge, in agreement with the arguments given in section 3 that finite ρ_* effects are less important for the core. Experiments on ASDEX Upgrade [91], in which the toroidal rotation is measured with high spatial resolution, show an inversion of the rotation profile in the outer 5 cm of the plasma, with the rotation profile exhibiting a local minimum around 1 cm inside the separatrix. This observation is consistent with a strong influence of the edge profiles on the local rotation, and furthermore indicates that the boundary condition on the rotation set at the separatrix is not likely to strongly influence the core rotation in H-mode plasmas. The edge residual stress scales with the local pressure gradient [90], consistent with a momentum flux driven by $E \times B$ shear connected with the edge pressure gradient, although alternative mechanisms like the neo-classical equilibrium [33] or the effect of profile shearing [75, 76] can have a similar scaling. Recent experiments on DIII-D and C-mod [92, 93] suggest a scaling of the pedestal rotation with the edge temperature gradient rather than the gradient of the pressure.

The link between momentum transport and ion heat transport has been observed on various machines and is well documented in the literature [8–17, 94]. This link is often expressed in an effective Prandtl number $Pr^\mathrm{eff} = \chi_\varphi^\mathrm{eff}/\chi_\mathrm{i}$, in which the effective diffusivity is defined to be the ratio of momentum flux (Γ_φ) and the gradient of the angular rotation ($nmR^2\nabla\Omega$). The effective Prandtl number is, therefore, not a direct measure of the momentum diffusivity, but contains contributions from the pinch as well as the residual stress. Experimentally obtained effective Prandtl numbers [17, 95–97] in the outer plasma region ($0.4 < r/a < 0.8$) are in the range $Pr^\mathrm{eff} \approx 0.1$–$0.4$, i.e. generally well below 1. Since higher values are expected for the diffusivity, the effective Prandtl numbers are indicative of a pinch or residual stress that moves momentum inwards, up the rotation gradient. A pinch contribution is proportional to the rotation rather than its gradient, and the effective Prandtl number is expected to be a function of the plasma rotation if the pinch leads to a substantial momentum flux. Indeed, experiments on JET in which the plasma rotation at the edge is reduced through the use of an enhanced toroidal ripple show an enhancement of the effective Prandtl number, reaching values close to 1 at the highest ripple strength [98]. The observation of peaked rotation profiles without momentum input [99, 100], of course, more directly proofs the existence of a pinch or residual stress.

The pinch contribution has been verified to exist in dedicated experiments. Modulation of the plasma torque

[14, 89, 101–107], and time evolution of the rotation profile after applying a magnetic perturbation that breaks the edge rotation [82, 108] allow for a separation of the diffusive and pinch contribution, and verify the existence of both. These experiments generally give Prandtl numbers in the range $Pr \approx 0.5$–2.5 [105–107] and pinch numbers $-R_a V_\varphi/\chi_\varphi \approx 1$–$6$ in rough agreement with the theoretical predictions. The parameter dependence of both transport coefficients has furthermore been studied. The increase in the pinch number $-R_a V_\varphi/\chi_\varphi$ with increased density peaking predicted by theory [57, 60] has been demonstrated [82, 89, 98, 109]. Also the weak dependence on collisionality predicted by theory [60, 65] has been experimentally verified [90, 109]. Although these observations are encouraging, other plasma parameter dependences have been reported [107] that appear difficult to explain theoretically.

The existence of the momentum flux generated through an up–down asymmetric magnetic equilibrium has been demonstrated through a dedicated experiment on the TCV tokamak [110, 111]. The unique plasma shaping capabilities of TCV allow for the generation of an equilibrium which has a large up–down asymmetry even in the confinement region. Furthermore, measurements of rotation without external momentum input are possible through the use of a diagnostic beam. The plasma shaping has been demonstrated to influence the gradient of the intrinsic rotation. Furthermore, the predicted change in sign of the momentum flux due to the up–down asymmetry with the direction of the magnetic field and plasma current, as well as through an up–down flip of the equilibrium, have all been demonstrated experimentally.

It is worth pointing out that effects other than turbulent transport can have a strong impact on the rotation profile. Sawteeth in the core of TCV have been shown to lead to flat or even hollow rotation profiles [112]. On JET also the edge localized modes (ELMs) have been found to have an impact [113]. The ELMs lead to larger losses of momentum compared with energy, resulting in a smaller plasma rotation at higher ELM frequency. Finally, scrape-off layer flows can determine the boundary condition of the rotation profile at the separatrix [46, 47].

The comparison between the theoretical predictions and experiments is encouraging, but many observations remain unexplained. Striking observations among the latter are the influence of electron heating or current drive [114–122], with central electron heating leading to a flattening in the rotation profile, the sudden transition in the rotation profile with an increase in density observed in TCV and C-mod [85, 86], and the apparent difference in behaviour between H-mode and EDH or ITBs [81, 123]. Also, for many observations the agreement is qualitative. Indeed, quantitative comparisons between experiments and direct numerical simulations are still relatively rare. Quasi-linear modelling efforts have been undertaken [109, 124, 125] for the diffusivity and the pinch. They show good agreement under some, but not all circumstances. It may be clear that a further quantitative comparison between experiments and direct numerical simulations is necessary to unravel the complex physics, and in order to make definite statements on the validity of the theory as well as the relevance of some of the proposed mechanisms.

6. Conclusions

Significant progress has been made in recent years on the understanding of momentum transport in tokamak plasmas. The lowest order ρ_* effects have been identified, and through the symmetry argument we know there are no other contributions at this order than the ones identified. A rough idea of their magnitude exists, and for some of the effects their interplay has been analysed. There is, however, a need for further exploration. The interplay between the various symmetry breaking mechanisms is insufficiently well understood. Determining the transport coefficients in a larger parameter range might perhaps not increase our physical insight, but will help to better understand how theory matches experimental observations. Furthermore, electro-magnetic effects and instabilities other than the ITG have hardly been touched upon. For the plasma core, linear calculations reveal that electro-magnetic effects might have an impact on the Prandtl number [50]. For the plasma edge the impact of electro-magnetic effects is expected to be significant [126]. The trapped electron mode has been studied in [65, 77], but certainly requires further study.

The situation is less clear for the momentum transport to higher order in ρ_*. Understanding these transport contributions is essential for the understanding of the edge as well as the core of some intrinsic rotation experiments. The theory, however, is not easy to track analytically, and a detailed computational investigation is challenging. Furthermore, for the edge of the plasma the lack in understanding of the H-mode barrier severely hinders the development of the theory. The way forward is undoubtedly the identification of those processes that dominate, rather than treating all possible processes. Dominant mechanisms in the edge are likely connected with the strong profile variation of density, temperature and potential, and possibly with the change in the equilibrium close to the X-point.

References

[1] Biglari H., Diamond P.H. and Terry P.W. 1990 *Phys. Fluids* B **2** 1
[2] Waltz R.E., Kerbel G.D., Milovich J. and Hammett G.W. 1995 *Phys. Plasmas* **2** 2408
[3] Bondeson A. *et al* 1994 *Phys. Rev. Lett.* **72** 2709
[4] Strait E.J. *et al* 1995 *Phys. Rev. Lett.* **74** 2483
[5] Peeters A.G. and Angioni C. 2005 *Phys. Plasmas* **12** 72515
[6] Kinsey J.E., Waltz R.E. and Candy J. 2005 *Phys. Plasmas* **12** 062302
[7] Roach C.M. *et al* 2009 *Plasma Phys. Control. Fusion* **51** 124020
[8] Suckewer S. *et al* 1981 *Nucl. Fusion* **21** 1301
[9] Burrell K. *et al* 1988 *Nucl. Fusion* **28** 3
[10] Weisen H. *et al* 1989 *Nucl. Fusion* **29** 2187
[11] Scott S.D. *et al* 1990 *Phys. Rev. Lett.* **64** 531
[12] Kallenbach A. *et al* 1991 *Plasma Phys. Control. Fusion* **33** 595
[13] Asakura N. *et al* 1993 *Nucl. Fusion* **33** 1165
[14] Nagashima K. *et al* 1994 *Nucl. Fusion* **34** 449
[15] Zastrow K.D. *et al* 1998 *Nucl. Fusion* **38** 257
[16] deGrassie J.S. *et al* 2003 *Nucl. Fusion* **43** 142
[17] Nishijima D. *et al* 2005 *Plasma Phys. Control. Fusion* **47** 89
[18] Mattor N. 1988 *Phys. Fluids* **31** 1180
[19] Eriksson L.-G. *et al* 1997 *Plasma Phys. Control. Fusion* **39** 27
[20] Rice J.E. *et al* 1998 *Nucl. Fusion* **38** 1
[21] Rice J.E. *et al* 1999 *Nucl. Fusion* **39** 1175

[22] Hutchinson I.H. *et al* 2000 *Phys. Rev. Lett.* **84** 3330
[23] Rice J.E. *et al* 2000 *Phys. Plasmas* **7** 1825
[24] Hoang G.T. *et al* 2000 *Nucl. Fusion* **40** 913
[25] deGrassie J.S. *et al* 2004 *Phys. Plasmas* **11** 4323
[26] Sakamoto Y. *et al* 2006 *Plasma Phys. Control. Fusion* **48** A63
[27] Scarabosio A. *et al* 2006 *Plasma Phys. Control. Fusion* **48** 663
[28] Bortolon A. 2006 *Phys. Rev. Lett.* **97** 235003
[29] Rice J.E. *et al* 2007 *Nucl. Fusion* **47** 1618
[30] Callen J.D. 2011 Effects of 3D magnetic perturbations on toroidal plasmas *Nucl. Fusion* **51** 094026
[31] Peeters A.G. 1998 *Phys. Plasmas* **5** 763
[32] Callen J.D. *et al* 2010 *Phys. Plasmas* **17** 056113
[33] Parra F.I. *et al* 2010 *Plasma Phys. Control. Fusion* **52** 045004
[34] Abiteboul J. *et al* 2010 *Proc. 37th EPS Conf. on Plasma Phys. (Dublin, Ireland, 21st June 2010)* (Vienna: European Physical Society) P1.1001 www.eps2010.com
[35] Scott B.D. *et al* 2010 *Phys. Plasmas* **17** 112302
[36] Denton R.E. and Kotschenreuther M. 1995 *J. Comput. Phys.* **119** 283
[37] Garbet X. *et al* 2010 *Nucl. Fusion* **50** 043002
[38] Parra F.I. *et al* 2011 *Phys. Plasmas* **18** 062501
[39] Dominguez R.R. and Staebler G.M. 1993 *Phys. Fluids* B **5** 3876
[40] Peeters A.G. *et al* 2004 *Phys. Plasmas* **11** 3748
[41] Peeters A.G. *et al* 2009 *Comput. Phys. Commun.* **180** 2650
[42] Waltz R.E., Kerbel G.D. and Milovich J. 1994 *Phys. Plasmas* **1** 2229
[43] Waltz R.E. *et al* 2007 *Phys. Plasmas* **14** 122507
[44] Casson F.J. *et al* 2009 *Phys. Plasmas* **16** 092303
[45] Peeters A.G. *et al* 2009 *Phys. Plasmas* **16** 042310
[46] LaBombard B. *et al* 2004 *Nucl. Fusion* **44** 1047
[47] LaBombard B. *et al* 2005 *Phys. Plasmas* **12** 056111
[48] Garbet X. *et al* 2002 *Phys. Plasmas* **9** 3893
[49] Gürcan Ö.D. *et al* 2007 *Phys. Plasmas* **14** 042306
[50] Strintzi D. *et al* 2008 *Phys. Plasmas* **15** 044502
[51] Weiland J. *et al* 2009 *Nucl. Fusion* **49** 065033
[52] Peeters A.G. *et al* 2006 *Plasma Phys. Control. Fusion* **48** B413
[53] Holod I. and Lin Z. 2008 *Phys. Plasmas* **15** 092302
[54] Holod I. and Lin Z. 2010 *Plasma Phys. Control. Fusion* **52** 035002
[55] Wang W.X. *et al* 2010 *Phys. Plasmas* **17** 072511
[56] Snodin A.P. *et al* 2011 Nonlinear gyro-kinetic flux tube simulations of the Prandtl number and Coriolis pinch effect *Phys. Plasmas* in preparation
[57] Peeters A.G. *et al* 2007 *Phys. Rev. Lett.* **98** 265003
[58] Hahm T.S. *et al* 2007 *Phys. Plasmas* **14** 072302
[59] Brizard A.J. 1995 *Phys. Plasmas* **2** 459
[60] Peeters A.G. *et al* 2009 *Phys. Plasmas* **16** 062311
[61] Peeters A.G. *et al* 2009 *Phys. Plasmas* **16** 034703
[62] Hahm T.S. *et al* 2008 *Phys. Plasmas* **15** 055902
[63] Gürcan Ö.D. *et al* 2008 *Phys. Rev. Lett.* **100** 135001
[64] Hein T. *et al* 2011 *Phys. Plasmas* **18** 072503
[65] Kluy N. *et al* 2009 *Phys. Plasmas* **16** 122302
[66] Angioni C. *et al* 2009 *Plasma Phys. Control. Fusion* **51** 124017
[67] Camenen Y. *et al* 2009 *Phys. Rev. Lett.* **102** 125001
[68] Camenen Y. *et al* 2009 *Phys. Plasmas* **16** 062501
[69] Staebler G.M. *et al* 2011 *Phys. Plasmas* **18** 056106
[70] Diamond P.H. *et al* 2008 *Phys. Plasmas* **15** 012303
[71] Gurcan O.D. *et al* 2010 *Phys. Plasmas* **17** 112309
[72] McDevitt C.J. *et al* 2009 *Phys. Rev. Lett* **103** 205003
[73] McDevitt C.J. *et al* 2009 *Phys. Plasmas* **16** 052302
[74] Gurcan O.D. *et al* 2010 *Phys. Plasmas* **17** 032509
[75] Camenen Y. *et al* 2011 *Nucl. Fusion* **51** 073039
[76] Waltz R.E. *et al* 2011 *Phys. Plasmas* **18** 042504
[77] Diamond P.H. *et al* 2009 *Nucl. Fusion* **49** 045002
[78] Kim J.Y. and Wakatani M. 1994 *Phys. Rev. Lett* **73** 2200
[79] Idomura Y., Ida M., Kano T., Aiba N. and Tokuda S. 2008 *Comput. Phys. Commun.* **179** 391
[80] Candy J. and Waltz R.E. 2003 *J. Comput. Phys.* **186** 545
[81] Rice J.E. *et al* 2004 *Phys. Plasmas* **11** 2427
[82] Kaye S.M. *et al* 2009 *Nucl. Fusion* **49** 045010
[83] Rice J.E. *et al* 2005 *Nucl. Fusion* **45** 251
[84] Rice J.E. *et al* 2008 *Plasma Phys. Control. Fusion* **50** 124042
[85] Duval B.P. *et al* 2007 *Plasma Phys. Control. Fusion* **49** B195
[86] Duval B.P. *et al* 2008 *Phys. Plasmas* **15** 056113
[87] Rice J.E. *et al* 2001 *Nucl. Fusion* **41** 277
[88] Solomon W.M. *et al* 2007 *Plasma Phys. Control. Fusion* **49** B313
[89] Solomon W.M. *et al* 2009 *Nucl. Fusion* **49** 085005
[90] Solomon W.M. *et al* 2010 *Phys. Plasmas* **17** 056108
[91] Putterich T. *et al* 2009 *Phys. Rev. Lett.* **102** 025001
[92] deGrassie J.S. *et al* 2009 *Nucl. Fusion* **49** 085020
[93] Rice J.E. *et al* 2010 *Proc. 23rd Int. Conf. on Fusion Energy 2010 (Daejeon, South Korea 2010)* (Vienna: IAEA) CD-ROM file EXC/3-3 and http://www-naweb.iaea.org/napc/physics/FEC/FEC2010/html/index.htm
[94] de Vries P.C. *et al* 2008 *Nucl. Fusion* **48** 065006
[95] de Vries P.C. *et al* 2006 *Plasma Phys. Control. Fusion* **48** 1693
[96] Tala T. *et al* 2007 *Nucl. Fusion* **47** 1012
[97] Tala T. *et al* 2007 *Plasma Phys. Control. Fusion* **49** B291
[98] de Vries P.C. *et al* 2010 *Plasma Phys. Control. Fusion* **52** 065004
[99] Lee W.D. *et al* 2003 *Phys. Rev. Lett.* **91** 205003
[100] Rice J.E. *et al* 2004 *Nucl. Fusion* **44** 379
[101] Ida K. *et al* 1995 *Phys. Rev. Lett.* **74** 1990
[102] Ida K. *et al* 1998 *J. Phys. Soc. Japan* **67** 4089
[103] Yoshida M. *et al* 2007 *Nucl. Fusion* **47** 856
[104] Yoshida M. *et al* 2008 *Phys. Rev. Lett.* **100** 105002
[105] Tala T. *et al* 2009 *Phys. Rev. Lett.* **102** 075001
[106] Tardini G. *et al* 2009 *Nucl. Fusion* **49** 085010
[107] Yoshida M. *et al* 2009 *Nucl. Fusion* **49** 115028
[108] Solomon W.M. 2008 *Phys. Rev. Lett.* **101** 065004
[109] Tala T. *et al* 2010 *Proc. 23rd Int. Conf. on Fusion Energy 2010 (Daejeon, South Korea 2010)* (Vienna: IAEA) CD-ROM file EXC/3-1 and http://www-naweb.iaea.org/napc/physics/FEC/FEC2010/html/index.htm
[110] Camenen Y. *et al* 2010 *Phys. Rev. Lett.* **105** 135003
[111] Camenen Y. *et al* 2010 *Plasma Phys. Control. Fusion* **52** 124037
[112] Sauter O. *et al* 2010 *Proc. 23rd Int. Conf. on Fusion Energy 2010 (Daejeon, South Korea 2010)* (Vienna: IAEA) CD-ROM file EXS/P2-17 and http://www-naweb.iaea.org/napc/physics/FEC/FEC2010/html/index.htm
[113] Versloot T.W. *et al* 2010 *Plasma Phys. Control. Fusion* **52** 045014
[114] Ida K. *et al* 2001 *Phys. Rev. Lett.* **86** 3040
[115] deGrassie J.S. 2004 *Phys. Plasmas* **11** 4323
[116] Manini A. *et al* 2006 *Nucl. Fusion* **46** 1047
[117] Ide S. *et al* 2007 *Nucl. Fusion* **47** 1499
[118] Degrassie J.S. *et al* 2007 *Phys. Plasmas* **14** 056115
[119] Rice J.E. *et al* 2009 *Nucl. Fusion* **49** 025004
[120] Ince-Cushman A. *et al* 2009 *Phys. Rev. Lett.* **102** 035002
[121] Yoshida M. *et al* 2009 *Phys. Rev. Lett.* **103** 065003
[122] McDermott R. *et al* 2011 *Plasma Phys. Control. Fusion* **53** 035007
[123] Fiore C.L. *et al* 2010 *Nucl. Fusion* **50** 064008
[124] Eriksson A. *et al* 2007 *Plasma Phys. Control. Fusion* **49** 1931
[125] Mantica P. *et al* 2010 *Phys. Plasmas* **17** 092505
[126] McDevitt C.J. *et al* 2009 *Phys. Plasmas* **16** 012301